1992

A numerical study of wind stress curl effects on eddies and filaments off the northwest coast of the Iberian Peninsula

Batteen, Mary L.

Elsevier Science Publishers B.V., Amsterdam

Journal of Marine Systems, 3 (1992) 249–266
Elsevier Science Publishers B.V., Amsterdam

A numerical study of wind stress curl effects on eddies and filaments off the northwest coast of the Iberian Peninsula

Mary L. Batteen, Carlos N. Lopes da Costa and Craig S. Nelson
Department of Oceanography, Naval Postgraduate School, Monterey, CA 93943-5000, USA

(Received December 1, 1990; revised version accepted August 2, 1991)

ABSTRACT

Batteen, M.L., Lopes da Costa, C.N. and Nelson, C.S., 1992. A numerical study of wind stress curl effects on eddies and filaments off the northwest coast of the Iberian Peninsula. J. Mar. Syst., 3: 249–266.

A high-resolution, multi-level, primitive equation ocean model is used to examine the response to the particular conditions of anticyclonic (negative) wind stress curl and equatorward (upwelling favorable) winds along the eastern ocean boundary off the northwest coast of the Iberian Peninsula in the vicinity of the highly productive rias. A band of steady equatorward winds, which are uniform alongshore but contain zonal variability (i.e., anticyclonic wind stress curl), results in an equatorward coastal surface current nearshore and a poleward surface current offshore. In time, the currents become unstable and lead to the development of anticyclonic warm core eddies. In addition, cold core filament formation occurs in areas where the anticyclones advect the upwelled coastal water offshore. The results from the experiments support the hypothesis that wind forcing, particularly the combination of anticyclonic (negative) wind stress curl and equatorward (upwelling favorable) winds, is an important mechanism for generating opposing alongshore surface currents, anticyclonic eddies, and filaments off the northwest coast of the Iberian Peninsula.

In a sensitivity study, the results from three numerical experiments are examined to understand, in a limited way, the dependence of the generation of the surface currents on the boundary conditions (free slip and no slip), the use of wind band forcing and the imposed wind stress curl distribution. Results show that, regardless of whether free-slip or no-slip boundary conditions or wind band forcing are used, opposing alongshore surface currents are generated. Because such currents do not develop when there is no wind stress curl, the opposing currents are generated by the anticyclonic wind stress curl.

Introduction

The eastern boundary current (EBC) system off the west coast of the Iberian Peninsula (IP), which extends from ~36° to 44°N, is on the northern fringe of the Canary Current coastal upwelling system, which extends from ~7.5°N (near Sierra Leone) to ~44°N (near Cape Finisterre), as shown in Fig. 1. The climatological winds are generally equatorward (upwelling favorable) off the IP during the spring and summer (e.g., Fig. 1b). The large-scale wind stress curl distribution during this same period (Fig. 1a) is characterized by nearshore regions of cyclonic wind stress curl which extend offshore ~200 km from the coast and anticyclonic wind stress curl further offshore in association with the anticyclonic circulation around the Azores High.

Based on one-degree (relatively large-scale) latitude/longitude climatological summaries of wind stress estimates derived from ship reports in the IP EBC region, and in other EBC (i.e., California, Peru/Humboldt, Benguela) regions, Bakun (1987) and Bakun and Nelson (1991) have shown the following: Cyclonic wind stress curl near the coast may result in divergent surface Ekman transport, upward Ekman pumping (oceanic upwelling) and poleward Sverdrup flow; conversely, anticyclonic wind stress curl in the offshore region may produce convergent Ekman

transport, downward Ekman pumping and equatorward Sverdrup flow. In addition to the effects of the curl on the ocean dynamics, the vertical transfers of both the physical and chemical properties associated with Ekman pumping may have major effects on the biological system. In particular, in EBC regions where the surface Ekman transport changes from divergent to convergent transport (i.e., near locations of zero wind stress curl contours), there may be significant physical/biological fronts formed with particularly high concentrations of oceanic food web organisms (which become rich feeding grounds for pelagic fish species, e.g., for tuna in the California Current System, according to Parrish et al., 1981). Unique to the northwest IP EBC region are the highly productive rias (e.g., for mussels, hake and other fish stocks), which are narrow indentations into the Galician coast of the IP, with a relatively unobstructed connection to the open ocean (Blanton et al., 1984). Recent, fine-scale (< 20 km spatial resolution) observations of local winds in the vicinity of these rias, have shown that "ria-induced" spatial variations in the wind stress curl significantly influences the flow within ~ 100 km of the coast in the northwestern region of the IP (Fraga, 1980; Blanton et al., 1984; McClain et al., 1986). For example, McClain et al. (1986) combined information on the wind stress derived from surface pressure analyses and ship wind

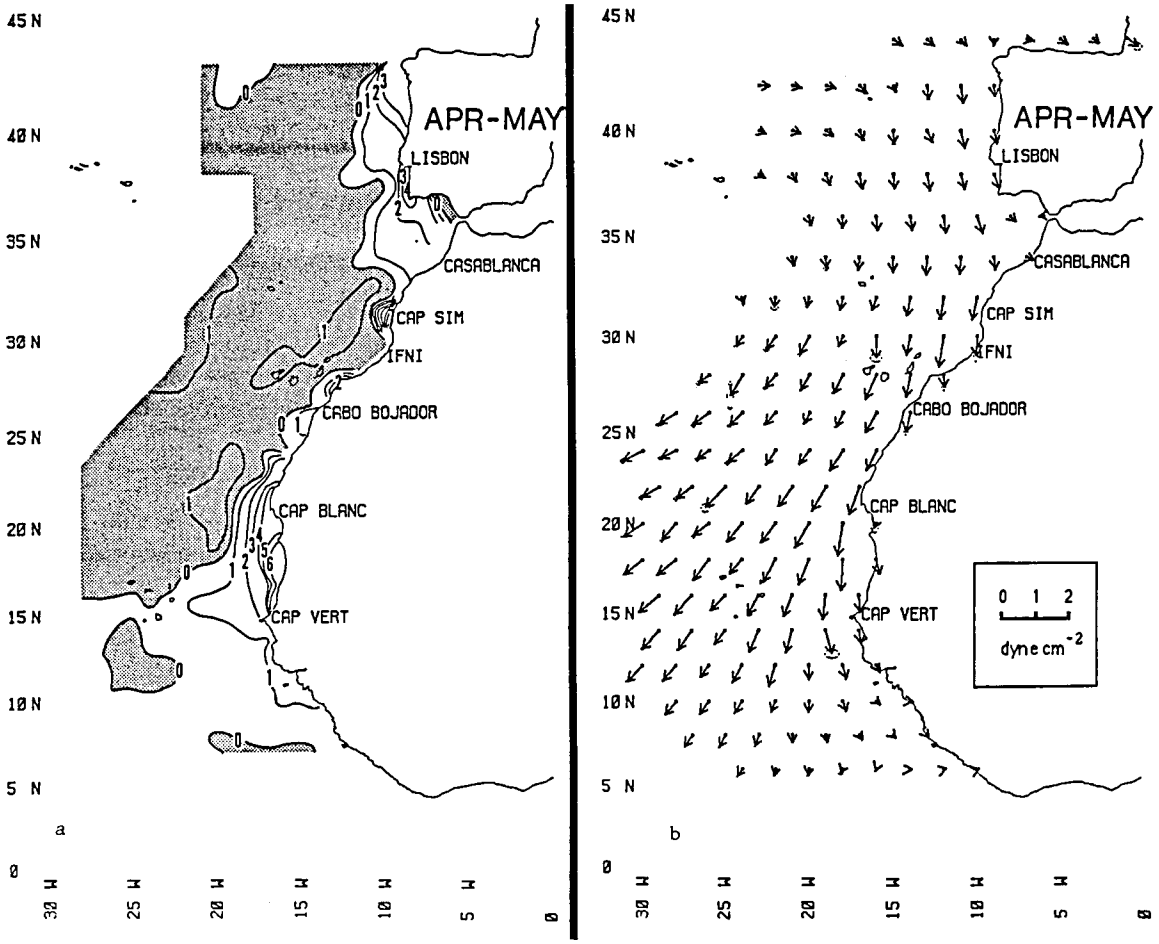

Fig. 1. Climatological wind stress curl (a) and wind stress (b) distributions for April-May in the area off the west coast of the Iberian Peninsula and Northwest Africa. Units are dynes/cm^2 per 1000 km in (a). Regions of anticyclonic wind stress curl are shaded and regions of cyclonic wind stress curl are unshaded (after Bakun and Nelson, 1991).

observations for the period from 18 to 22 April 1982 and found consistently stronger winds with a heading to the southwest at the mouth of Ria de Arosa (~ 42.5°N), parallel to the axis of the ria, and generally weaker winds offshore. McClain et al. (1986) concluded that the existence of the resulting large anticyclonic (negative) wind stress curl could be a primary driving mechanism for the current shear associated with an observed southward coastal jet adjacent to a northward current offshore.

Recent observations have shown that, superimposed on the broader-scale, EBC system of the IP, are highly energetic, mesoscale features. In particular, satellite images of the sea surface temperature distribution off Portugal and northwest Spain, taken during periods of winds favorable for upwelling, have shown evidence of cold water plumes or filaments extending offshore and mesoscale eddies with horizontal dimensions of order ~ 100 km (Fiuza, 1983, 1984; Fiuza and Sousa, 1989). In other EBC regions, particularly in the California Current System, filaments and eddies have also been observed during periods of winds favorable for upwelling. These observations provide evidence for wind forcing as a possible important mechanism for the formation of currents, eddies and filaments in EBC regions.

Because the role of wind forcing in the generation of eddies and filaments in the IP has not been systematically explored, the primary objective of this study is to investigate the combination of anticyclonic (negative) wind stress curl and upwelling favorable winds as a possible generation mechanism for the coastal currents, eddies and filaments in the EBC region off the northwest coast of the IP. A high-resolution, multilevel, primitive equation (PE) model is used to examine the response to climatological wind forcing in the EBC region off the IP. A band of steady, equatorward (upwelling favorable) winds, which are uniform alongshore but contain zonal variability (i.e., anticyclonic wind stress curl) is used as forcing in the PE model. It is shown that, consistent with McClain et al. (1986), anticyclonic wind stress curl is a significant generation mechanism for opposing alongshore coastal surface currents in the nearshore region. In addition, we extend the results of McClain et al. (1986) by showing that the currents are unstable and as a result, eddies and filaments are generated.

The organization of the study is as follows. In the second section the PE ocean model and the experimental conditions used in the study are described. In the third section the results of the model simulations along with an analysis of the results are shown. The results of model sensitivity studies are presented in the fourth section and a summary is presented in the last section.

The model

Model description

To investigate the role of steady climatological wind forcing on the IP ocean circulation, the wind stress fields, discussed below, were used to specify the wind forcing for a high-resolution, multi-level, PE model of a baroclinic ocean on a β-plane. The model is based on the hydrostatic, Boussinesq, and rigid lid approximations. The governing equations are defined in Batteen et al. (1989). For the finite differencing, a space-staggered B-scheme (Arakawa and Lamb, 1977; Batteen and Han, 1981) is used in the horizontal. In the vertical, the 10 layers are separated by constant z levels at depths of 13, 46, 98, 182, 316, 529, 870, 1416, 2283 and 3656 m. Although it is known that continental margins and bottom topography can strongly influence both the large-scale currents and eddy dynamics (e.g., Warren, 1963; Holland, 1967; 1973; Orlanski and Cox, 1975; Rhines, 1977), a flat bottom boundary condition is imposed in this process-oriented, wind forcing study. The constant depth used in the model is 4500 m.

The eastern boundary of the model domain is closed, and, to isolate the role of wind forcing in the generation of eddies, is modeled as a straight, vertical wall. The kinematic boundary condition of no flow through the boundary is imposed on the cross-shore component. Either free-slip or no-slip boundary conditions can be applied on the alongshore velocity component. In the main experiment, a no-slip condition on the alongshore

velocity is invoked. In a sensitivity study (see the fourth section), we will examine the effects of no-slip versus free-slip conditions on an eastern boundary, because the impact of the boundary conditions has been shown by Blandford (1971) to be significant in western boundary current circu-

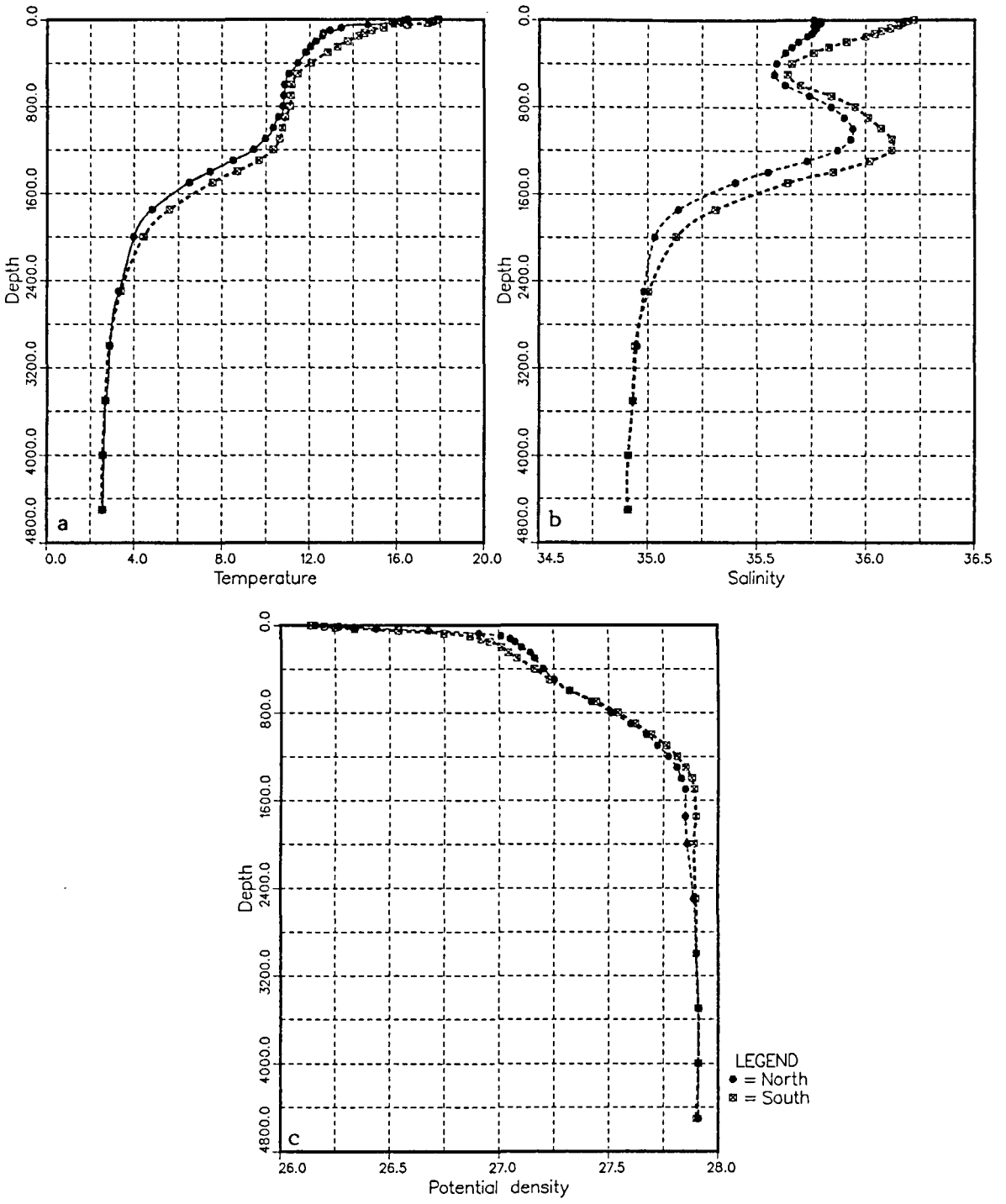

Fig. 2. Climatological profiles of (a) temperature, (b) salinity and (c) potential density for 5-degree latitude/longitude quadrangles centered at 42.5° N, 12.5° W and 37.5° N, 12.5° W. The units for temperature, salinity, potential density, and depth are °C, ppt, kg m^{-3} and meters, respectively. Data are from Levitus (1982).

lations. The northern, southern and western borders are open boundaries which use a modified version of the radiation boundary conditions of Camerlengo and O'Brien (1980). The model domain covers the western coast of the IP region, from ~35° to 44°N (1024 km alongshore) and from ~9° to 15°W (512 km cross-shore). Horizontal resolution of the model is 16 km alongshore and 8 km cross-shore.

The model uses biharmonic lateral heat and momentum diffusion with the same choice of coefficients (i.e., 2.0×10^{17} cm^4 s^{-1}) as in Batteen et al. (1989). Holland (1978) showed that the highly scale-selective biharmonic diffusion acts predominantly on sub-mesoscales, while Holland and Batteen (1986) found that baroclinic mesoscale processes can be damped by Laplacian lateral heat diffusion. As a result, the use of biharmonic lateral diffusion should allow mesoscale eddy generation via barotropic (horizontal shear) and/or baroclinic (vertical shear) instability mechanisms. As in Batteen et al. (1989), weak (0.5 cm^2 s^{-1}) vertical eddy viscosities and conductivities are used. Bottom stress is parameterized by a simplified quadratic drag law (Weatherly, 1972), as in Batteen et al. (1989).

The initial temperature field

A comparison of climatological profiles of temperature, salinity and potential density (Fig. 2a–2c, respectively) from Levitus (1982) from the IP region shows that temperature effects dominate salinity effects in the upper water column (above ~600 m depth). Because the primary effects of wind forcing should be limited to the upper depths, we neglected salinity effects in this experiment. Based on the mean climatological temperature profile (Fig. 2a) from Levitus (1982) for the 5° latitude/longitude square centered at 37.5° N, 12.5°W, a simplified approximation was used to initialize the temperature field in the model. This approximation consisted of using exponential fits to the climatological profile for the upper 500 m and the lower 3300 m of the water column, with a linear variation between. The

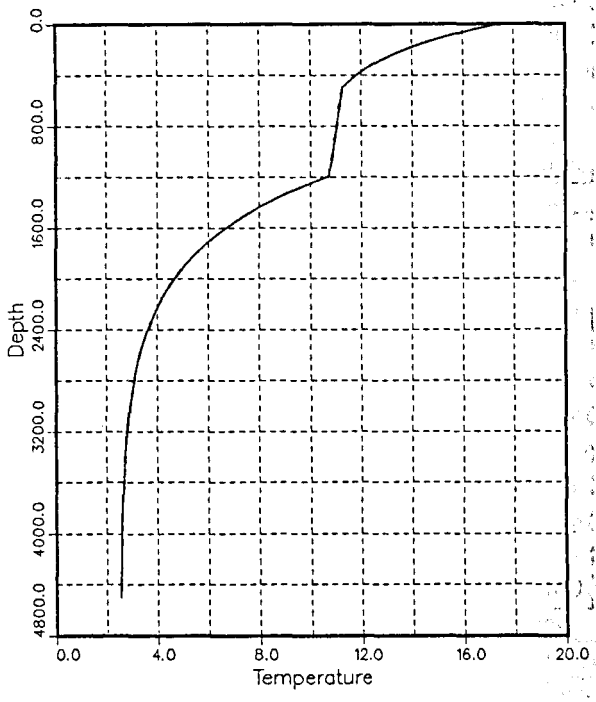

Fig. 3. Initial temperature profile used in the model. Units for depth and temperature are meters and °C, respectively.

function, which fits the climatological profile of Levitus (1982) shown in Fig. 2a, is given by:

$$T(z) = 9.8 + 7.7\, e^{(z/300)}, \quad (-500\ \text{m} \leqslant z \leqslant 0\ \text{m})$$
$$T(z) = 11.25 + 7.857 \times 10^{-4}(z + 500), \quad (-1200\ \text{m} \leqslant z \leqslant -500\ \text{m})$$
$$T(z) = 2.5 + 8.2\, e^{\left(\frac{(z+1200)}{600}\right)}, \quad (-4500\ \text{m} \leqslant -1200\ \text{m}) \qquad (1)$$

The resulting temperature profile (Fig. 3) was used to provide initial values at each of the 10 levels in the model.

Wind forcing

McClain et al. (1986) studied the flow field off the west coast of the IP forced by a negative wind stress curl in the vicinity of rias. The diagrams of the applied wind forcing and the resulting current velocity field and interfacial displacements for the McClain et al. (1986) experiment, are shown in Figs. 4a,b, respectively. The southward flow adjacent to the west coast was driven by the southward coastal wind, while the northward flow offshore was associated with the negative curl of the wind stress (McClain et al., 1986). A similar type of structure in the wind field is used as the forcing in our experiment for the coastal study region (within ~ 65 km of the coast) off the IP (Fig. 5). In the regions offshore, the climatological wind field, based on Bakun and Nelson's (1991) wind stress distributions (Fig. 1) for the IP during the upwelling season, is used as the forcing.

The resulting equatorward wind forcing used in the model (Fig. 5) consists of uniform (i.e.,

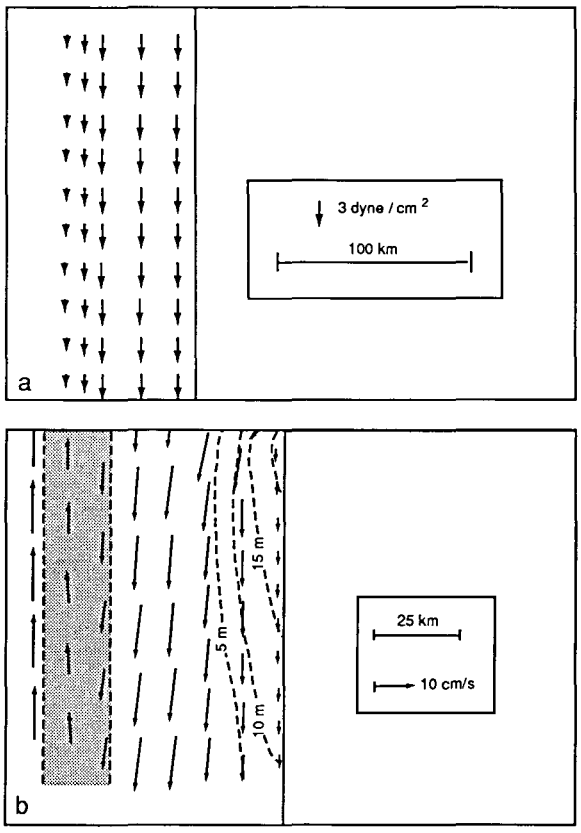

Fig. 4. (a) Numerical model geometry and the specified southward wind field applied in the simulation of McClain et al. (1986). (b) The flow field and pycnocline displacement resulting from the wind forcing shown in (a). Dashed lines are lines of constant displacement of the interface, and the shaded area defines the area of strong negative wind stress curl. The maximum wind stress is 3 dynes/cm^2 (adapted from McClain et al., 1986).

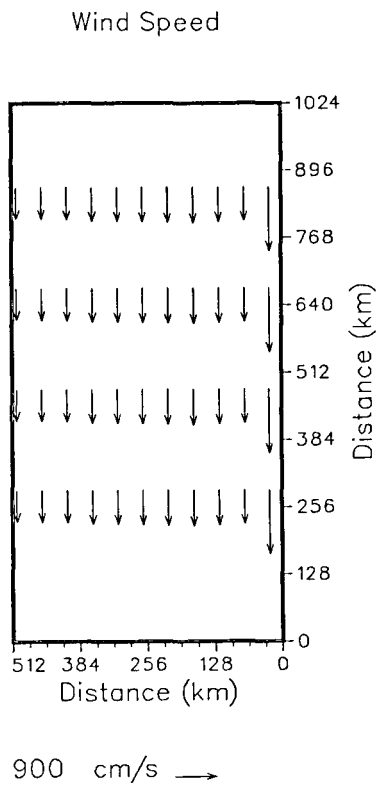

Fig. 5. Imposed wind forcing for the study region off the Iberian Peninsula. To avoid clutter, the wind vectors are plotted at every fifteenth gridpoint in the alongshore direction, at every sixth gridpoint in the cross-shore direction, and velocities less than 50 cm/s are not plotted. The maximum wind speed is 1425 cm/s (~ 3 dynes/cm^2).

curl-free) equatorward wind stress within ~ 50 km of the coast; negative (anticyclonic) wind stress curl in the band between ~ 50 and ~ 65 km from the coast; positive (cyclonic) wind stress curl between ~ 65 and 185 km; and negative (anticyclonic) wind stress curl offshore of 185 km. To isolate the effects of this particular wind forcing, the winds change only in the cross-shore direction and are steady in time. To establish a baseline for the effects of negative wind stress curl, we will examine the effects of wind stress forcing with and without curl in a sensitivity study (see fourth section). In addition, all wind forcing is imposed in the interior only and drops to zero near the northern and southern open boundaries, consistent with the wind band forcing used by McCreary et al. (1987) and Batteen et al. (1989). In a sensitivity study (see fourth section), we will compare the effects of wind forcing imposed throughout the model domain with the effects of wind band forcing.

The thermal forcing

The eastern boundary region off the west coast of the IP has, in the mean, a net heat gain from April through September, i.e., coincident with the upwelling season (Bakun, 1987). This net gain occurs because of relatively low cloud cover (compared with further offshore), reduced latent heat flux, and downward sensible heat flux in the coastal region, due to the presence of cold, upwelled water during summer. To focus this study on wind forcing as a possible mechanism for the generation of thermal variability in the IP, the surface thermal forcing in the model was highly simplified. The incoming solar radiation at the top of the atmosphere Q_0, was specified to the 983.3 cal cm^{-2} day^{-1} (List, 1963), as representative for June and July at latitude 39.5°N. The sum of the net long-wave radiation, latent heat and sensible heat fluxes, Q_B, was computed during the model experiments from standard bulk formulas (Haney et al., 1978), using April through September mean values of cloud cover, relative humidity, surface atmospheric pressure, the model simulated sea surface temperature, and the specified wind speed and air temperature. Climatological (April through September) values for cloud cover, relative humidity and surface atmospheric pressure of 0.48, 86% and 1018.3 mb, respectively, were taken from the climatological atlas by Esbenson and Kushnir (1981). The initial air temperature of 289°K was chosen to produce a zero net heat flux across the surface, i.e., the total heat flux was initially set to zero by specifying an initial air temperature which forced the net flux of long-wave radiation, sensible heat and latent heat to zero. As a result, any subsequent surface heat flux forcing is a secondary effect of the changes in sea surface temperature due to the wind forcing. As discussed in Haney (1985), such a surface thermal forcing damps the sea surface temperature fluctuations to the

atmosphere on a time scale of the order of 100 days. Consequently, sea surface temperature fluctuations that develop due to wind forcing should be observed long before they are damped by the computed heat flux.

Results

Here we examine the oceanic response to wind forcing in the EBC region of the IP, and analyze the dynamical reasons for the generation of the

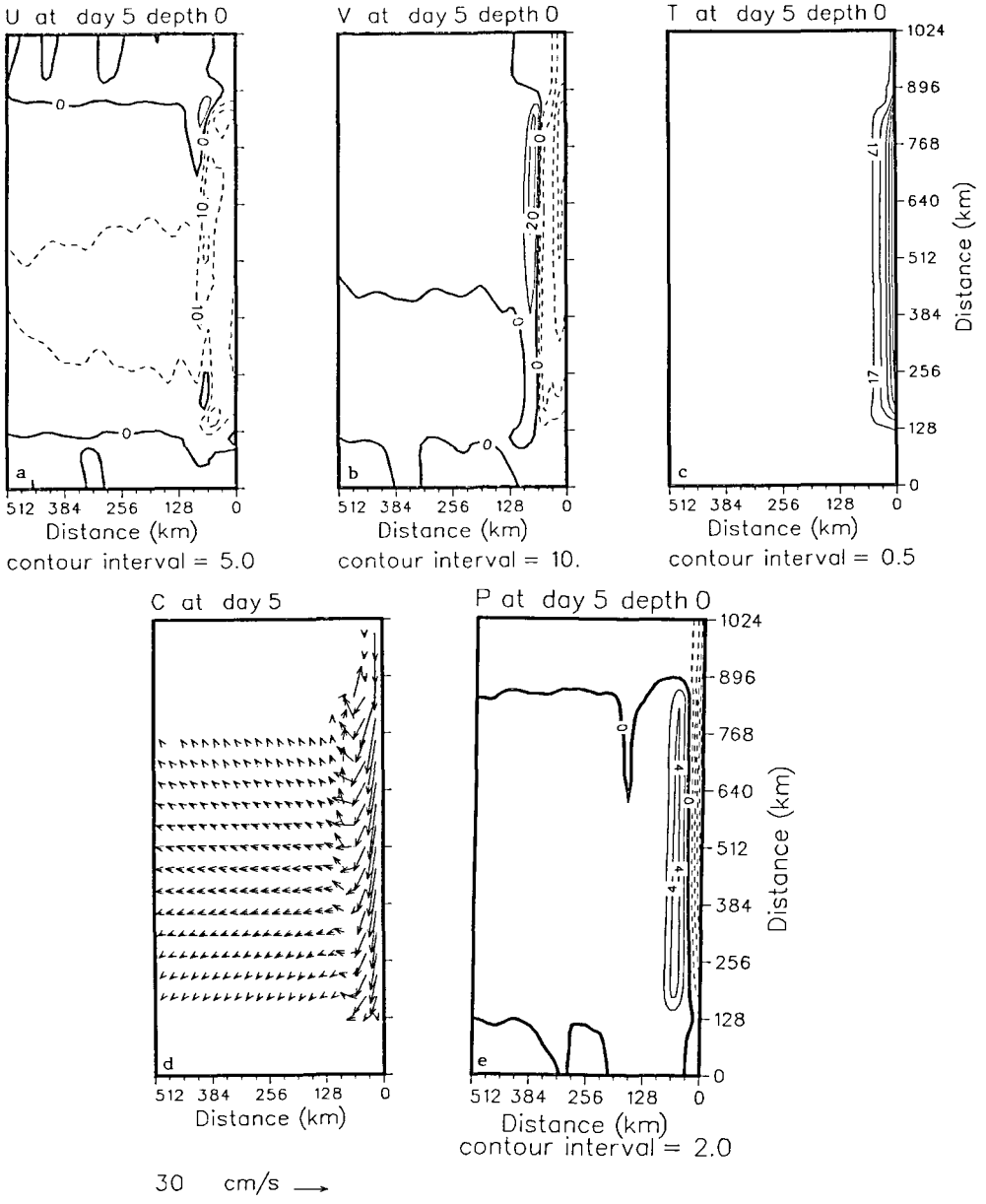

Fig. 6. Surface isopleths at day 5 of (a) zonal velocity, (b) meridional velocity, (c) temperature, (d) velocity vectors, and (e) dynamic height relative to 2400 m depth. The contour interval is 5 cm/s for (a), 10 cm/s for (b), 0.5°C for (c), and 2 cm for (e). Dashed lines denote offshore velocities in (a), equatorward velocities in (b), and negative values relative to 2400 m depth in (e). In both the velocity vector fields presented (Figures 6d and 10b), to avoid clutter, velocity vectors are plotted at every third gridpoint in both the cross-shore and alongshore directions, and velocities less than 2 cm/s are not plotted.

particular oceanic features which develop. Results for a 40-day model simulation period will be shown, since this was a sufficient time to allow for the generation of currents, eddies and filaments.

Development of the coastal jet and offshore countercurrent

The model was forced with full magnitude winds and, as expected, inertial oscillations developed in the near-surface currents. These oscillations were damped after several inertial periods. By day 5, a westward surface flow (Figs. 6a,d) results, due to offshore Ekman transport, as expected. The largest negative values (magnitudes > 10 cm/s) for the flow are seen in a meridional band with its axis located ~ 60 km from the coast. A cross-section taken in the middle of the domain (Fig. 7a) elucidates the surface temperature structure (Fig. 6c) and shows that the upper ocean isotherms slope downward toward the coast at distances between ~ 82 and 57 km from the coast and slope upward within ~ 57 km of the coast. The upwelled isotherms near the coast are consistent with a divergence of the flow in the Ekman layer under the influence of the equatorward, coastal wind with a compensating vertical motion to replace the surface water. Farther offshore, decreasing velocities of the equatorward wind decreases the offshore Ekman transport, resulting in surface layer convergence and downwelling, consistent with the pattern of isotherms seen in Fig. 7a. The region of imposed negative wind stress curl (distances from the coast between 48 and 64 km) coincides with the locations of both the ridge in the surface dynamic height field (Fig. 6e) and the change in sign of the slopes of the upper ocean isotherms. The pressure gradient force, due to the surface slope and horizontal gradient of temperature (density), changes in sign across this region of negative wind stress curl so that an equatorward surface jet results within approximately 55–60 km from the coast and a poleward surface jet appears offshore (Fig. 6b). This is clearly identified in a vertical cross-shore section of the meridional velocity field (Fig. 7b), which shows the separation between the opposing jets at ~ 60 km from the coast. The equatorward jet has a maximum velocity of ~ 15–30 cm/s at ~ 10 km from the coast, and a vertical extent of ~ 300 m. The surface poleward jet offshore has a

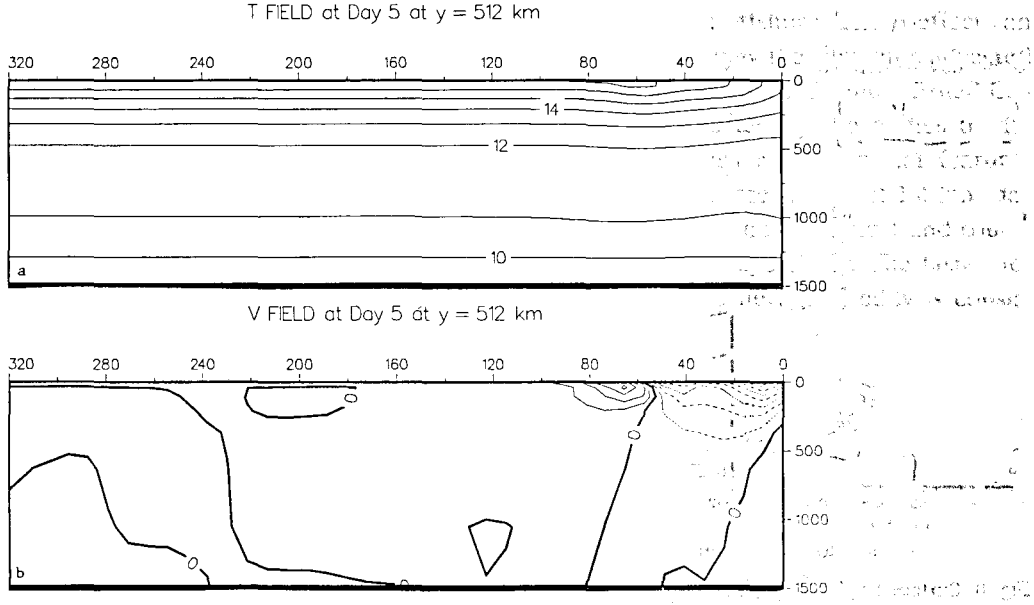

Fig. 7. Vertical cross-shore section at day 5 of (a) temperature and (b) meridional velocity. Contour interval is 1°C in (a) and 5 cm/s in (b). Dashed lines in (b) denote equatorward flow. The vertical cross-sections were taken at $y = 512$ km, in the middle of the model domain.

maximum velocity of ~ 15–20 cm/s at ~ 70 km from the coast and a vertical extent of ~ 200 m. Results of this experiment on day 5 are qualitatively consistent with the results of McClain et al. (1986), in which the currents forced by a similar wind field reached a maximum southward speed of ~ 15 cm/s, shoreward of the wind shear zone, and a maximum northward speed of ~ 15 cm/s offshore of this zone.

The generation of eddies

By day 20, the coastal equatorward surface jet, within 60 km of the coast, has intensified to a maximum alongshore-average speed of ~ 60 cm/s. The surface poleward jet offshore also has an increased maximum alongshore average speed of ~ 20–40 cm/s. Superimposed on the dominant poleward and equatorward surface jets (Fig. 8b) are eddies, as seen in the surface zonal current field (Fig. 8a) at $y \sim 190$ and 735 km. These perturbations are confined to within ~ 120 km of the coast in the same region as the poleward and equatorward jets.

Following Batteen et al. (1989), we investigate the necessary conditions for instability by examining the distribution of potential velocity, q, in time-averaged cross-sections of the coastal flow.

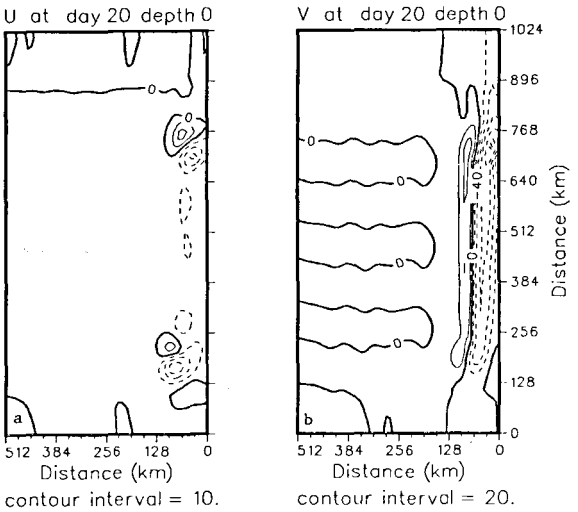

Fig. 8. Surface isopleths of (a) zonal velocity and (b) meridional velocity at day 20. Contour interval is 10 cm/s in (a) and 20 cm/s in (b). Dashed lines denote offshore and equatorward velocities in (a) and (b), respectively.

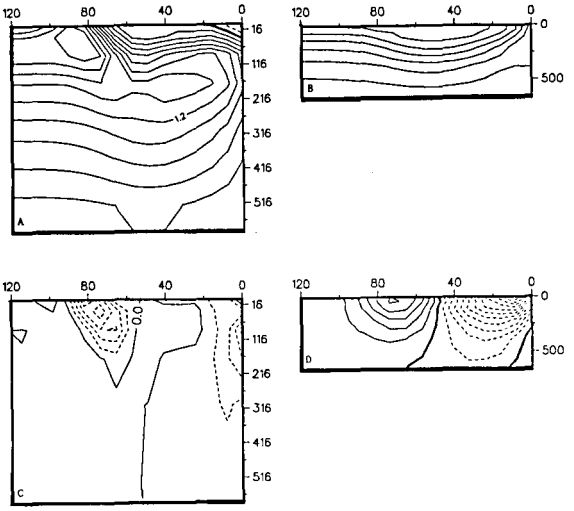

Fig. 9. Vertical cross-sections for the time-averaged days 21–30 of (a) potential vorticity, (b) temperature, (c) the cross-stream derivative of potential vorticity multiplied by the zonal grid size (°C/m s) and (d) meridional velocity. Values are scaled by 10^6. Contour interval is 0.2°C/(m s) in (a), 1.0°C in (b), 0.1°C/(m s) in (c) and 10 cm/s in (d). Dashed contours denote negative values in (c) and (d). The vertical cross-sections were taken at $y = 736$ km.

Following Watts (1983), the potential vorticity, q, may be approximated by the expression:

$$q = (f + \zeta)\frac{\partial T}{\partial z} - \frac{\partial T}{\partial x}\frac{\partial v}{\partial z}, \qquad (2)$$

where

$$\zeta = \frac{\partial v}{\partial x} - \frac{\partial u}{\partial y}.$$

A cross-section of the time-averaged (days 21–30) potential vorticity at $y = 736$ km, is shown in Fig. 9a. The choice of days 21 through 30 for the time averaging corresponds to the period in which the instabilities developed. Away from the upper layers of the coastal region, there is a tendency for potential vorticity to be uniform along isothermal surfaces and to change vertically, consistent with the temperature stratification (Fig. 9b). A relative maximum of potential vorticity is present at a depth of about 150 m, corresponding to the seasonal thermocline (i.e., the maximum vertical gradient of temperature). In the upper ocean, within ~ 120 km of the coast, the distribution of isolines of potential vorticity is complicated by large horizontal gradients of meridional velocity (Fig. 9d).

The cross-stream derivative of potential vorticity [calculated by computing the horizontal derivative $(\partial q/\partial x)$ and then multiplying by one grid length (δx)] changes sign in the upper ocean (Fig. 9c), at a distance of ~ 45 km from the coast, corresponding well to the axis where anticyclonic eddies are generated in the experiment. Comparison of the potential vorticity gradient (Fig. 9c) with the alongshore velocity (Fig. 9d) shows that the product of the two fields is positive at some location in the domain, which satisfies the necessary condition for barotropic instability (Kamenkovich et al., 1986). As a result, barotropic instability is likely the main mechanism for the generation of the anticyclones in this experiment.

The eddy fields

By day 40, the surface temperature and velocity vector fields (Fig. 10a,b) show the existence of four, well developed, warm-core, anticyclonic eddies with center positions at $y \sim 252$, 438, 604 and 755 km. Because the centers of the eddies nearly coincide with the zone of large negative wind stress curl, the four anticyclonic circulations are likely generated by the anticyclonic shear of the wind in this region. The three northernmost eddies have circular patterns, with diameters of ~ 150 km, while the southern eddy has an elliptical pattern, with its major axis oriented northeast/southwest. All of the eddies have warm cores (consistent with warm core rings) as seen in Figs. 10a and 11 for the eddy located at $y \sim 624$ km. The near-surface isotherms associated with the eddies show considerable downward displacements. For instance, as shown in Fig. 11, the 17°C isotherm surrounds the eddy at the surface and is

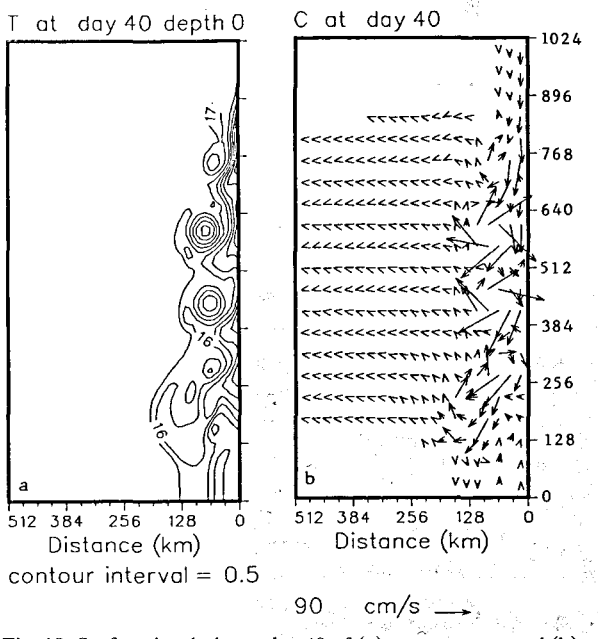

Fig. 10. Surface isopleths at day 40 of (a) temperature and (b) velocity vector fields. Contour interval is 0.5°C in (a).

displaced downward to ~ 200 m depth. The surface temperature pattern (Fig. 10a) also shows four cold water filaments corresponding to locations where the circulation associated with each of the four anticyclones advects the upwelled coastal water offshore. The southern filament is the largest, advecting relatively cold water (below 15°C) as far as 185 km offshore. The β-effect can be invoked to explain why the filaments advected by the southernmost eddies extend farther offshore than those advected by the eddies to the north. The anticyclones advect coastal features westward at estimated rates of about 1.4 km/day and 2.3 km/day for the northernmost and southernmost anticyclones, respectively. The faster advection rate of the southernmost eddy is consis-

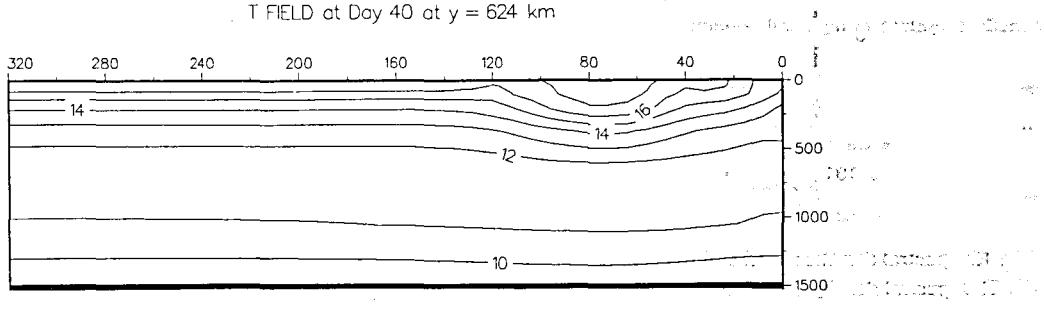

Fig. 11. Vertical cross-shore section of temperature at $y = 624$ km at day 40. Contour interval is 1°C.

tent with a β-induced motion, i.e., β is larger at lower latitudes.

To estimate the dominant wavelengths at which eddy growth occurs, a spectral analysis technique was used. The spectral densities of the fluctuations of u, v and T associated with the alongshore component wave number are shown in Fig. 12. The spectral densities were computed by sampling the fields at the model grid points (for the upper level and for the alongshore region between 32 km and 256 km offshore) corresponding to the region with the most eddy activity. Notice

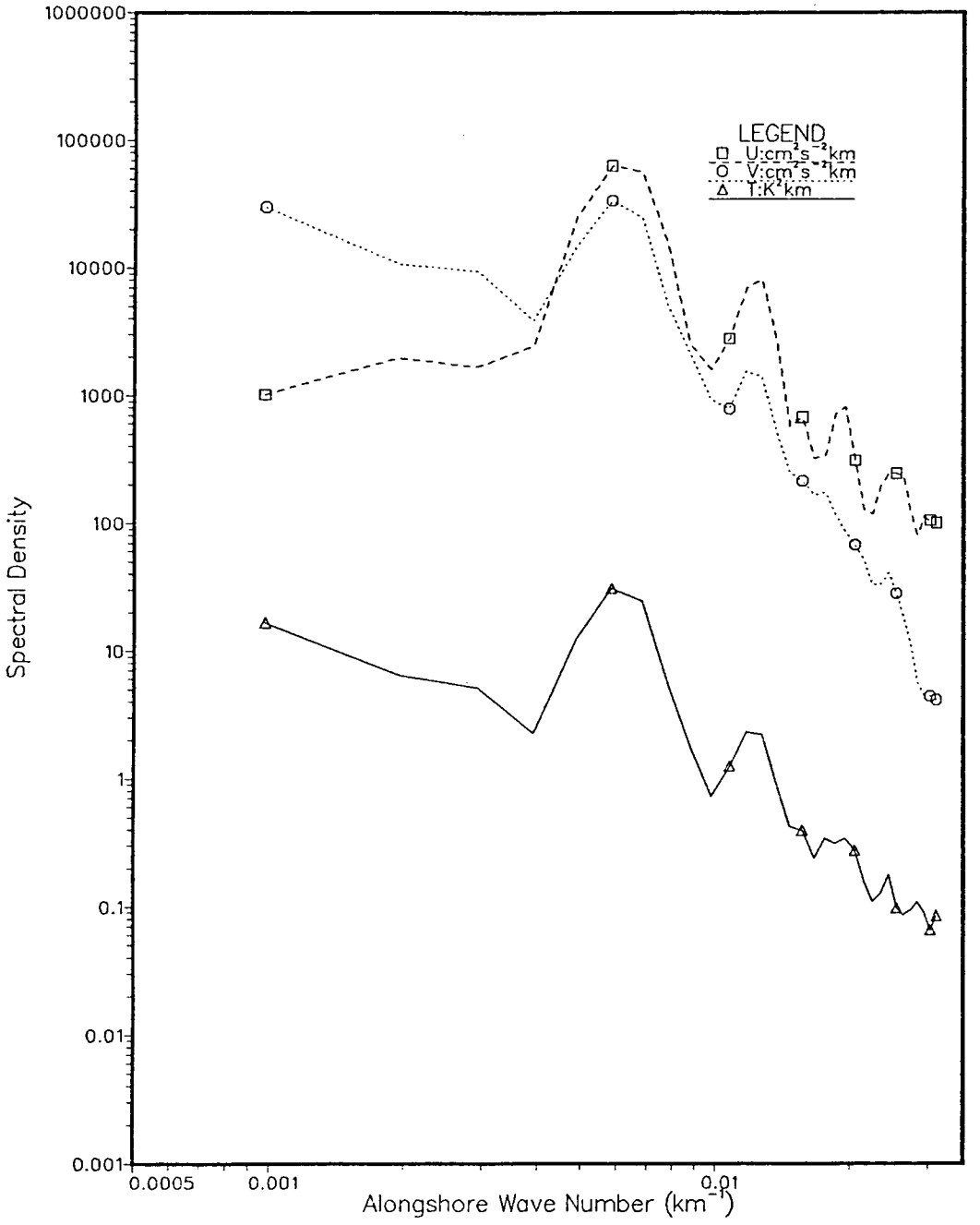

Fig. 12. Spectral densities for the alongshore wave number of zonal (u) velocity, meridional (v) velocity and temperature (T) at day 40. The spectral density estimates were obtained from the spatial series of variables u, v, and T for the alongshore region between 32 km and 256 km offshore. Units of spectral densities are $cm^2\ s^{-1}$ km for u and v and K^2 km for T.

that the peaks of the spectra for u, v and T show the same alongshore spatial scales. The dominant meridional wave number is ~ 0.0055 km^{-1}, which corresponds to a wavelength of ~ 180 km. This agrees with the scales of the eddies seen in the surface temperature field (Fig. 10a).

Sensitivity studies

In this section, results from three additional numerical experiments are examined to understand, in a limited way, the sensitivity of the model results described in the previous section to the boundary condition (free slip and no slip), use of wind band forcing and wind stress curl. To facilitate discussion of the results, Table 1 shows the four experiments (including the basic case discussed in the previous section, which we call Experiment 1) and the choices for the several parameters.

Like other model sensitivity studies (e.g., Holland and Lin, 1975a,b), the basic approach in carrying out these experiments has been to change only one parameter for each case. By comparing and contrasting the results of each experiment with the results of the basic case, we gain a better understanding of the importance of each parameter.

The effect of boundary conditions (Experiments 1 and 2)

In both experiments, the kinematic boundary condition of no flow through the eastern boundary was imposed on the cross-shore velocity component. In the main experiment, Experiment 1, a no-slip condition on the alongshore velocity was imposed. In experiment 2 the effect of a free-slip boundary condition is investigated. All other model parameters are the same as in Experiment 1.

The flow patterns in Experiment 2 (Fig. 13b) are quite similar to Experiment 1 (Fig. 13a). For example, as shown by the vertical cross-section of the meridional velocity at day 20 in the middle of the model domain, in both cases there is a surface-intensified, coastal, equatorward jet within ~ 60 km of the coast with a maximum core speed of ~ 60 cm/s. Offshore there is a surface-intensified, poleward jet with a maximum core speed of ~ 40 cm/s at ~ 80 km from the coast. Between ~ 250 and 600 m depth, there is a relatively weak (~ 6 cm/s) and narrow, poleward undercurrent at the coast.

The temperature patterns in both cases (Fig. 13e,f) are also similar. Consistent with coastal upwelling due to equatorward winds, the upper ocean isotherms slope upward in the vicinity of the equatorward, coastal jet. Near the coast, in the vicinity of the poleward undercurrent, the isotherms slope downward, as expected. Offshore, in the region of the surface, poleward jet, the isotherms also bend downward, consistent with downwelling due to the imposed anticyclonic wind stress curl pattern.

Because the impact of no-slip versus free-slip conditions has been shown by Blandford (1971) to be severe in other (particularly, western) boundary current circulations, it may at first be surprising to see similar results for both cases. Two explanations for the similarities can be given. The first explanation is that, even though the free-slip

TABLE 1

The boundary conditions, types of wind forcing, and use of wind band forcing for the experiments discussed in section 4. Blanks indicate no change from Experiment 1

Parameters				
Experiment number	Boundary conditions	Type of wind forcing	Wind band forcing used?	Remarks
1	no slip	wind stress curl	yes	basic model
2	free slip			
3			no	
4		wind stress with no curl		

condition causes an input of positive vorticity at the eastern boundary (compare Fig. 14a,b in the upper, coastal layers), which could lead to a significant vorticity contribution, the input of negative vorticity offshore at ~80 km at the coast (Fig. 14a,b) used in both cases is much larger than that due to the boundary conditions. As a result, significant currents develop offshore in response to the wind forcing and not due to vorticity input at the eastern boundary.

The second explanation, based on the grid-point model configuration near the coastal boundary, relates large changes in the velocity field to spurious momentum leaks. In particular, if the boundary of the grid lies on momentum grid points, as in Bryan (1963) and a no-slip condition is imposed, there will be no lateral momentum leaks. In contrast, with the same placement of momentum grid-points on the boundary, if a free-slip boundary condition is

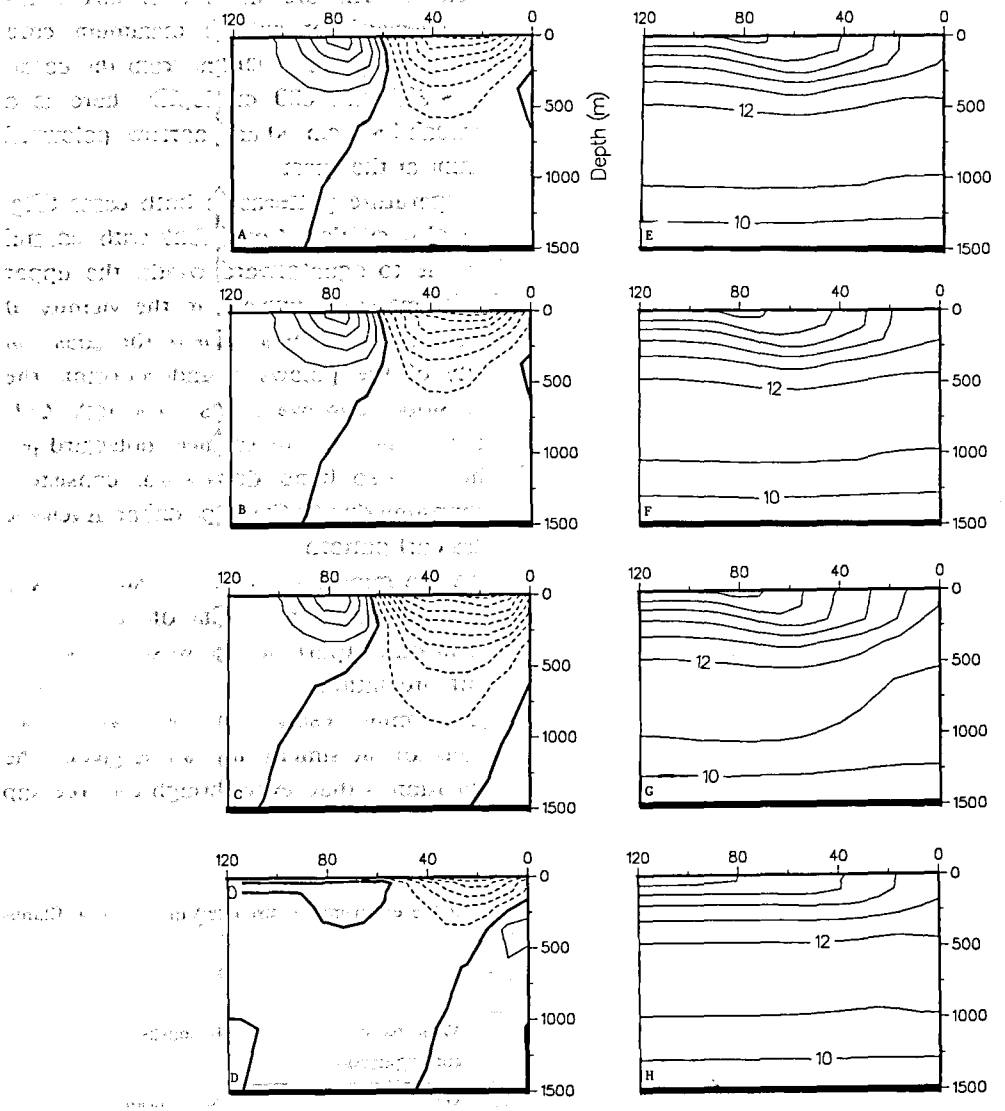

Fig. 13. Vertical cross-shore sections at day 20 of meridional velocity (a–d) and temperature (e–h) for Experiments 1 (a,e), 2 (b,f), 3 (c,g) and 4(d,g). Contour interval is 10 cm/s in (a–d) and 1°C in (e–h). Dashed lines in (a–d) denote equatorward flow. The vertical cross-sections were taken at $y = 512$ km.

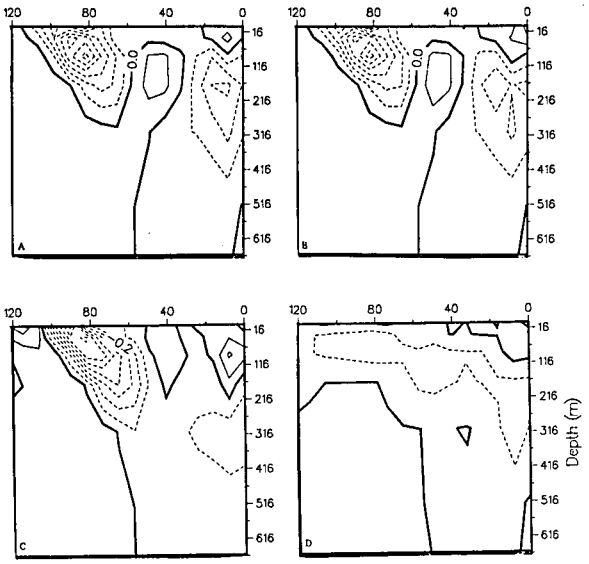

Fig. 14. Vertical cross-sections for the time-averaged days 21–30 of the cross-stream derivative of potential vorticity multiplied by the zonal grid size (°C/m s) for Experiments 1 (a), 2 (b), 3 (c) and 4 (d). Values are scaled by 10^6. Contour interval is 0.1°C/(m s). Dashed contours denote negative values. The vertical cross-sections were taken at $y = 512$ km.

used, there can be lateral momentum leaks which, according to Semtner and Mintz (1977), could distort the nonlinear circulation.

In this study, as in Haney (1974) and Semtner and Mintz (1977), the horizontal velocity and temperature grid points are staggered in the horizontal and the boundary of the grid lies on the temperature points. This avoids possible lateral momentum leaks. It also allows either free- or no-slip boundary conditions to be invoked, without violating kinetic energy conservation principles.

Use of wind band forcing (Experiment 3)

This experiment shows the effect of applying the wind forcing not only in the interior but also on the northern and southern open boundaries of the model domain. The flow, temperature and vorticity patterns in Experiment 3 are quite different below the surface layers than in Experiment 1. In particular, the equatorward, coastal jet developed in Experiment 3 (Fig. 13c) is much stronger and deeper than the jet which was generated in Experiment 1 (Fig. 13a). This deep, strong, equatorward flow also dominates the coastal, subsurface region where a poleward undercurrent developed in Experiment 1. Consistent with the flow pattern, the isotherms in Experiment 3 (Fig. 13g) bend upward from deeper depths near the coast and individual isotherms outcrop at the surface further from the coast than in Experiment 1. The core of the input of positive vorticity in the coastal region is also displaced deeper i.e., from ~15 to 50 m depth (compare Fig. 14a,c).

An explanation for the different effects which can be attributed to wind band forcing is as follows: If there is no alongshore variability in either the wind forcing or pressure gradient field (as in Experiment 3), no undercurrent will be generated. Instead, a coastal, alongshore current will develop that is too strong, too deep and oriented in the direction of the alongshore component of the wind stress at all depths. These results are similar to those obtained by McCreary (1981) under similar conditions. To generate a relatively realistic undercurrent, he recommended the use of wind band forcing (similar to that used in Experiment 1), which imposes an alongshore variability in the wind forcing. The use of wind band forcing, while somewhat artificial in nature, allows for the propagation of coastal Kelvin waves which thereby establish the alongshore pressure gradient field, with the result that a surface-trapped coastal jet and a relatively realistic undercurrent are generated.

Wind stress with no curl (Experiment 4)

To establish a baseline for the effects of wind stress curl, we examine the results of the model, driven by equatorward wind forcing with and without curl. In Experiment 4, a steady, uniform (curl-free) equatorward wind stress of ~3.5 dynes/cm^2 is used as the forcing. The flow (Fig. 13a,d), temperature (Fig. 13e,h) and vorticity patterns (Fig. 14a,d) in Experiments 1 and 4 show similar results only in the region within ~50 km of the coast, as expected, because there is no curl in this region in either experiment. In both cases, the model response is that expected from the divergence of offshore transport and upwelling in

the immediate vicinity of the coastal boundary. Offshore, the oceanic response seen in Experiment 1 is clearly due to the presence of the strong, negative wind stress curl and not to the equatorward wind stress. This response, which is not evident in Experiment 4, consists of a poleward flow (Fig. 13a), a downward bending of isotherms (Fig. 13e) and enhanced vertical and horizontal gradients in the vorticity field (Fig. 14a).

Summary

This study used a high-resolution, multi-level, primitive equation (PE) ocean model to investigate the role of climatological wind forcing as a possible generation mechanism for the coastal current, filaments, and eddies in the eastern boundary current (EBC) region off the northwest coast of the Iberian Peninsula (IP). A band of steady equatorward winds, uniform alongshore but with zonal variability (i.e., wind stress curl), was used as the forcing.

By day 5, in the meridional band of negative wind stress curl, there was a change in sign of the zonal gradients of surface velocity, of surface dynamic height and of the upper ocean temperature field. The upwelled isotherms near the coast were consistent with vertical motion required to compensate the Ekman layer divergence due to the equatorward, coastal winds. Further offshore, in the region of negative wind stress curl (due to the decreased equatorward winds), the offshore Ekman transport was reduced, resulting in surface layer convergence and downwelling. As expected, the distribution of the surface dynamic heights relative to 2400 m (which are proportional to temperature) showed a meridionally extended ridge in the band of negative wind stress curl. The equatorward surface current nearshore and poleward surface current offshore of the ridge were approximately in geostrophic balance with the pressure gradient forces due to the horizontal distribution of density. The ridge of dynamic height parallel to the coast which balances the equatorward flow nearshore and poleward flow offshore was consistent with the expected response to upper layer convergence driven by the anticyclonic wind stress curl overlying the ridge.

By day 20, both equatorward and poleward surface currents had intensified. There was evidence of eddies at $y \sim 190$ and 735 km superimposed on this system. By day 40, four, well-developed anticyclonic, warm core eddies were present along a meridional axis located close to the band of negative wind stress curl. All eddies were likely generated due to a barotropic (horizontal shear) instability process resulting from the anticyclonic shear of the wind in this region. The subsequent breaking up of the ridge due to the instability process would leave remnants of high dynamic heights that would constitute anticyclonic eddies. The alongshore wavelength of the eddies was estimated, based on spectral analysis, to be ~ 180 km. Cold water filaments were discernible in places where the circulation of each anticyclone advected the upwelled water offshore.

In a sensitivity study, the results from three numerical experiments were examined to understand, in a limited way, the dependence of the generation of the surface currents on the boundary conditions (free-slip and no-slip), the use of wind band forcing and the wind stress curl. Results showed that, regardless of whether free-slip or no-slip boundary conditions or wind band forcing were used, opposing alongshore surface currents were generated. Because such currents did not develop when there was no wind stress curl, the opposing currents were generated due to the anticyclonic wind stress curl.

Both the equatorward nearshore surface current and poleward surface countercurrent offshore, reproduced early in the experiment, were qualitatively consistent with a similar numerical experiment (McClain et al., 1986) and with observations of northward transport nearshore, as indicated by Coastal Zone Color Scanner (CZCS) imagery off the west coast of the IP (e.g., McClain et al., 1986; Fiuza and Sousa, 1989). While ship wind reports provide some evidence for the negative wind stress curl pattern off the west coast of Galicia in the vicinity of rias, no available observations exist to verify how persistent or how far downstream of the northwest coast of the IP this negative wind stress curl feature may occur.

The results from this experiment support the hypothesis that wind forcing, particularly the combination of anticyclonic (negative) wind stress curl and equatorward (upwelling favorable) winds, is an important generation mechanism of the currents, anticyclonic eddies and upwelling filaments observed off the west coast of the IP. However, such a combination cannot occur year-round, since during the fall and winter the upwelling favorable winds reverse or weaken. According to Haynes and Barton (1990), when the equatorward trade winds, characteristic of the summer months, weaken or reverse, poleward flow should be generated by thermohaline forcing off the coast of the IP.

It should also be noted that this process-oriented study employed the constraints of a regular, straight coastline and a flat bottom to isolate and examine the effects of wind forcing. Features like the irregular coastline and bottom topography associated with the IP will be included in future studies because they are likely to be important mechanisms in controlling the locations of mesoscale features, as suggested by the satellite imagery of Fiuza and Sousa (1989), and in generating current shear. Inclusion of salinity, which is important in controlling the density at the depths of the Mediterranean Water influence, may also improve the accuracy of the results in the numerical experiments. Besides the numerical studies, observational programs on the shelf and slope should be implemented, including current meter arrays, Lagrangian current drifters, remote sensing and hydrographic surveys with appropriate space/time resolution to synoptically map mesoscale structures. Such a program would allow more realistic comparisons with the numerical studies.

The results of this study may also be applicable to other EBC areas which have the combination of regions of negative wind stress curl and upwelling favorable winds near the coast. Examples of such regions are the EBC areas off Baja California and Northwest Africa (see Fig. 1a, for example), which can be identified by persistent lobes of anticyclonic curl extending from the offshore regions into the coast (Bakun and Nelson, 1991). Due to the association of the curl in these regions with both large-scale frontal boundaries and high mesoscale activity (Bakun, 1987), the wind stress curl in these regions may have major effects on both the ocean dynamics (as demonstrated in this study) and on the biological system.

Acknowledgments

This work was supported by direct funding at the Naval Postgraduate School (NPS) with the Office of Naval Research as the sponsor. Computer resources were provided by the W.R. Church Computer Center at NPS. The authors wish to thank the anonymous reviewers, whose helpful comments led to a much improved manuscript.

References

Arakawa, A. and Lamb, V.R., 1977. Computational design of the basic dynamical processes of the UCLA general circulation model. in: J. Chang (Editor), Methods Comput. Phys., 17: 173–265.

Bakun, A., 1987. Applications of maritime data to the study of surface forcing of seasonal and interannual ocean variability in eastern boundary regions. Ph.D. Diss. Oregon State Univ., Corvallis, OR, 226 pp.

Bakun, A. and Nelson, C.S., 1991. The seasonal cycle of wind stress curl in subtropical eastern boundary current regions. J. Phys. Oceanogr., in press.

Batteen, M.L. and Han, Y.-J., 1981. On the computational noise of finite-difference schemes used in ocean models. Tellus, 33: 387–396.

Batteen, M.L., Haney, R.L., Tielking, T.A. and Renaud, P.G., 1989. A numerical study of wind forcing of eddies and jets in the California Current System. J. Mar. Res., 47: 493–523.

Blandford, R.R., 1971. Boundary conditions in homogeneous ocean models. Deep-Sea Res., 18: 739–751.

Blanton, J.O., Atkinson, L.P., Fernandez de Castillejo, F. and Lavin Montero, A., 1984. Coastal upwelling off the Rias Bajas, Galicia Northwest Spain. 1. Hydrographic studies. Rapp. P.-V. Reun. Cons. Int. Explor. Mer, 183: 79–90.

Bryan, K., 1963. A numerical investigation of a nonlinear model of a wind-driven ocean. J. Atmos. Sci., 20: 594–606.

Camerlengo, A.L. and O'Brien, J.J., 1980. Open boundary conditions in rotating fluids. J. Comput. Phys., 35: 12–35.

Esbenson, S.K. and Kushnir, Y., 1981. The heat budget of the global ocean: an atlas based on estimates from surface marine observations. Climatic Res. Inst. Rep., 29, 27 pp.

Fiúza, A.F.G., 1983. Upwelling patterns off Portugal. In: E. Suess and J. Thiede (Editors), Coastal Upwelling. Its Sediment Record. Plenum Press, New York, pp. 85–97.

Fiúza, A.F.G., 1984. Hidrologia e dinâmica das àguas costeiras de Portugal. Dissertação apresentada à Universidade de Lisboa para obtenção do grau de Doutor em Física, especialização em Ciências Geofísicas. Univ. Lisboa, 294 pp.

Fiúza, A.F.G. and Sousa, F.M., 1989, Preliminary results of a CTD survey in the Coastal Transition Zone off Portugal during 1-9 September 1988. Coastal Transition Zone Newsl., 4: 2–9.

Fraga, F., 1980. Upwelling off the Galician coast, Northwest Spain. In: F.A. Richards (Editor), Coastal Upwelling. Am. Geophys. Union, Washington, D.C., pp. 176–182.

Haney, R.L., 1974. A numerical study of the response of an idealized ocean to largescale surface heat and momentum flux. J. Phys. Oceanogr., 4: 145–167.

Haney, R.L., 1985. Midlatitude sea surface anomalies: A numerical hindcast. J. Phys. Oceanogr., 15: 787–799.

Haney, R.L., Shiver, W.S. and Hunt, K.H., 1978. A dynamical-numerical study of the formation and evolution of large-scale ocean anomalies. J. Phys. Oceanogr., 8: 952–969.

Haynes, R. and Barton, E.D., 1990. A poleward flow along the Atlantic coast of the Iberian peninsula. J. Geophys. Res., 95: 11, 425–11, 441.

Holland, W.R., 1967. On the wind-driven circulation in an ocean with bottom topography. Tellus, 19: 582–599.

Holland, W.R., 1973. Baroclinic and topographic influences on the transport in western boundary currents. Geophys. Fluid Dyn., 4: 187–210.

Holland, W.R., 1978. The role of mesoscale eddies in the general circulation of the ocean—Numerical experiments using a wind-driven quasi-geostrophic model. J. Phys. Oceanogr., 8: 363–392.

Holland, W.R. and Lin, L.B., 1975a. On the generation of mesoscale eddies and their contribution to the oceanic general circulation. I. A preliminary numerical experiment. J. Phys. Oceanogr., 5: 642–657.

Holland, W.R. and Lin, L.B., 1975b. On the generation of mesoscale eddies and their contribution of the oceanic general circulation. II. A parameter study. J. Phys. Oceanogr., 5: 658–669.

Holland, W.R. and Batteen, M.L., 1986. The parameterization of subgrid scale heat diffusion in eddy-resolved ocean circulation models. J. Phys. Oceanogr., 16: 200–206.

Kamenkovich, V.M., Koshlyakov, M.N. and Monin, A.S., 1986. Synoptic Eddies in the Ocean. D. Reidel, Dordrecht, 433 pp.

Levitus, S., 1982. Climatological atlas of the world ocean. U.S. Dep. Commer. NOAA Prof. Pap., 13, 173 pp.

List, R.J., 1963. Smithsonian Meteorological Tables. Smithsonian Inst., Washington, D.C., 527 pp.

McClain, C.R., Chao, S., Atkinson, L.P., Blanton, J.O. and Castillejo, F., 1986. Winddriven upwelling in the vicinity of Cape Finisterre, Spain. J. Geophys. Res., 91: 8470–8486.

McCreary, J.P., 1981. A linear stratified ocean model of the coastal undercurrent. Philos. Trans. R. Soc. London, A 302: 385–413.

McCreary, J.P., Kundu, P.K. and Chao, S., 1987. On the dynamics of the California Current System. J. Mar. Res., 45: 1–32.

Orlanski, I. and Cox, M.D., 1973. Baroclinic instability in ocean currents. Geophys. Fluid Dyn., 4: 297–332.

Parrish, R.H., Nelson, C.S. and Bakun, A., 1981. Transport mechanisms and reproductive success of fishes in the California Current. Biol. Oceanogr., 1: 175–203.

Rhines, P.B., 1977. The dynamics of unsteady currents. In: E.D. Goldberg, I.N. McCave, J.J. O'Brien and J.H. Steele (Editors), Wiley, New York, pp. 519–548.

Semtner, A.J. and Mintz, Y., 1977. Numerical simulation of the Gulf Stream and mid-ocean eddies. J. Phys. Oceanogr., 7: 208–230.

Warren, B.A., 1963. Topographical influences on the path of the Gulf Stream. Tellus, 16 167–183.

Watts, D.R., 1983. Gulf stream variability. In: A.R. Robinson (Editor), Eddies in Marine Science. Springer, New York, pp. 114–144.

Weatherley, G.L., 1972. A study of the bottom boundary layer of the Florida current. J. Phys. Oceanogr., 2: 54–72.